

RESEARCH

Open Access



Preoperative assessment in lymph node metastasis of pancreatic ductal adenocarcinoma: a transformer model based on dual-energy CT

Xia Ding^{2†}, Wei Xu^{1†}, Yan Xu³, Yongchuang Zhang¹, Huaxiao Xu¹, Lin Guo¹ and Lei Li^{1,4*}

Abstract

Background Deep learning(DL) models can improve significantly discrimination of lymph node metastasis(LNM) of pancreatic ductal adenocarcinoma(PDAC), but have not been systematically assessed.

Purpose To develop and test a transformer model utilizing dual-energy computed tomography (DECT) for predicting LNM in patients with PDAC.

Materials and methods This retrospective study examined patients who had undergone surgical resection and had pathologically confirmed PDAC, with DECT performed between August 2016 and October 2022. Six predictive models were constructed: a DECT report model, a clinical model, 100 keV DL model, 150 keV DL model, a combined 100 + 150 keV DL model, and a model that integrated clinical information with DL-derived signatures. Multivariable logistic regression analysis was employed to develop the integrated model. The efficacy of these models was assessed by comparing their areas under the receiver operating characteristic curve (AUC) using the DeLong test. Survival analysis was conducted using Kaplan-Meier curves.

Results In brief, 223 patients (mean age, 57 years \pm 11 standard deviation; 93 men) were evaluated. All patients were divided into training ($n = 160$) and test ($n = 63$) sets. Patients with LNM accounted for 96 of the 223 patients (43%). In the test set, the integrated model, which integrated DECT parameters such as IC and Z, CA-199 levels, DECT reports, and DL signatures, demonstrated the highest performance in predicting LNM, with an AUC of 0.93. In contrast, the radiologists' assessment and the clinical model yielded AUCs of 0.60 and 0.62, respectively. The integrated model-predicted positive LNM was associated with worse overall survival (hazard ratio, 1.75; 95% confidence interval: 1.22 - 2.83; $P = .023$).

Conclusion A transformer-based model outperformed radiologists and clinical model for prediction of LNM at DECT in patients with PDAC.

[†]Xia Ding and Wei Xu co-first authors contributed equally to this manuscript.

*Correspondence:

Lei Li

369542019@qq.com

Full list of author information is available at the end of the article



Key points

- An integrated nomogram incorporating dual-energy computed tomography (DECT) parameters such as iodine concentration (IC) and effective atomic number (Z), carbohydrate antigen-199 levels, DECT imaging reports, and deep learning signatures demonstrated superior predictive accuracy for lymph node metastasis (LNM) in patients with pancreatic ductal adenocarcinoma (PDAC), achieving an area under the receiver operating characteristic curve (AUC) of 0.93 in the test set.
- This nomogram significantly outperformed both the radiologists' reports and the clinical model in predicting LNM in PDAC cases.

Keywords Lymph node metastasis, Pancreatic ductal adenocarcinoma, Deep learning, Dual-energy computed tomography, Progression-free survival

Summary

A nomogram based on dual-energy computed tomography, utilizing a transformer model, significantly outperformed both radiologists and clinical models in predicting lymph node metastasis in patients with pancreatic ductal adenocarcinoma.

Introduction

By 2030 years, as the most common pancreatic malignant tumor, pancreatic ductal adenocarcinoma (PDAC) may become the second leading cause of cancer mortality in the United States [1, 2]. To date, increasingly advanced surgical protocols and chemotherapeutic regimens were used to PDAC patients, but their final outcomes remain dismal with less than 15% of 5-years survival rate [3, 4]. Lymph node metastasis (LNM) plays a crucially important role in patients with PDAC underwent R0 resection. Therefore, international guidelines (e.g. the European Society for Medical Oncology [ESMO] and national Comprehensive Cancer Network [NCCN], etc.) recommended neoadjuvant treatment (NAT) to the LNM positive population, being contributed to improve long-term survival after surgery [5–7].

Although the pathological result obtained preoperatively from puncture biopsy is still used as the gold standard in clinical practice, it is limited by the invasive nature and the possibility of severe damage to the complex pancreatic glandular region. High-quality, multi-slice spiral computed tomography (CT) is the main imaging examination for PDAC, but it faced enormous challenge to distinguish between metastasis and inflammatory reactions of an enlarged LN. A meta-analysis reported that using CT to distinguish LNM of PDAC provided a low performance with 25% sensitivity and 28% accuracy [8–10]. To enhance the spatial contrast of the pancreatic region, dual-energy computed tomography (DECT) has been developed, involving the acquisition of CT attenuation data at two energy levels to enlarge spatial resolution between soft tissues [11–13]. Moreover,

multi-parameters of DECT including CT value derived from virtual monoenergetic image (VMI) 40 keV and 70 keV, K value, electron cloud density (Rho), and effective atomic number (Z), etc. both help radiologists identifying the occupying lesions.

Previously, our team have reported that DECT model based on ResNet18 algorithm could identify precisely LNM before surgery, providing an outstanding prognostic stratification of PDAC patients [14]. Notably, Vaswani et al. report that a transformer architecture as a special DL model that primarily designed for sequence-to-sequence tasks based on a self-attention mechanism to capture dependencies between input and output elements [15], has been used increasingly to predict oncological outcomes. For example, Wentao Wang et al. reported that using transformer-based network for prediction of microvascular invasion of HCC patients [16]. But there is currently no developed transformer model for prediction of LNM in patients with PDAC.

Therefore, the aim of our study was to develop and test a transformer-based model based on DECT to distinguish LNM of PDAC. Our findings will give an accurate and non-invasive method to adjust therapeutic schemes for PDAC.

Materials and methods

This retrospective study complied with the Transparent Reporting of a Multivariable Prediction Model for Individual Prognosis or Diagnosis (TRIPOD) guideline [17] and obtained approval of the institutional review board (B2019 -012-01) following the principles of the 1975 Helsinki Declaration. All written informed consent was waived due to its retrospective nature.

Study sets

Between August 2016 and October 2022, 1,258 consecutive patients with PDAC underwent surgery with standard regional lymph node dissection were identified from two high-volume institutions according

to the following eligibility criteria: (i) the nature of tumors and adjacent enlarged lymph nodes were pathologically confirmed; (ii) preoperatively diagnosed as respectable complied with the American Joint Committee on Cancer TNM staging, and (iii) all PDAC patients received DECT scanning within two weeks before surgery. Patients were excluded if they: (i) had any malignancies other than PDAC; (ii) missing DECT imaging for reliable assessment; and (iii) lost follow-up. NAT, including chemoradiation therapy or cytotoxic chemotherapy, was executed in some patients. Figure 1. shows the enrolment pathway of PDAC patients. Finally, a total of 223 patients were enrolled at two tertiary referral hospitals. We selected 160 eligible patients in Qingdao Central Hospital into the training set and other 63 in Air Force Medical Center were assigned into test set, respectively.

The histologic examination of tumor specimens was performed by two pathologists (W.W, 10 years' experience and L.W.L.,10 years' experience) through serially examining LNM.

DECT Image protocol

All PDAC patients were scanned using a third-generation dual-source DECT machine Siemens dual-source CT (SOMATOM Force CT, SIEMENS, Germany), and the scan range was from the top of the diaphragm to the bifurcation of the abdominal aorta. We used the software Synovia VB10B for the multi-parameter analysis of the energy spectrum. The DECT technique and postprocessing are shown in Supplementary Materials E1.1–1.2. Dual-energy parameters were measured by placing a region of interest (ROI) of tumor and pancreatic region. The collection and definition of clinical variables, DECT parameters and pathological findings were shown in Supplementary Materials E1.3.

Follow-up

Per patient who received surgery were regularly followed up using serum carbohydrate antigen (CA)- 199 and contrast enhanced imaging after 1 month and every 3–6 months thereafter. Two fellowship-trained abdominal radiologists were assigned into assessment in pancreatic

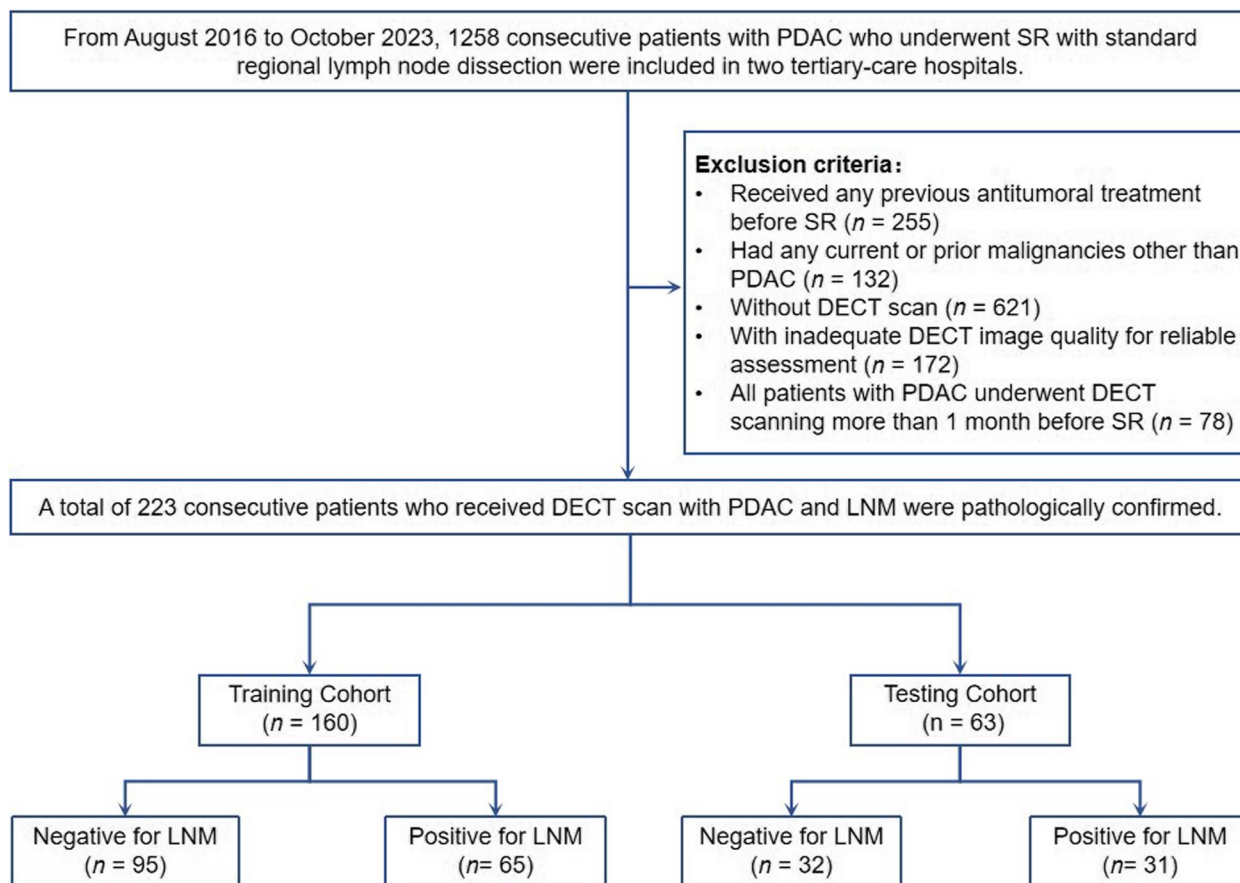


Fig. 1 Flowchart depicting the enrollment pathway of patients with Pancreatic Ductal Adenocarcinoma (PDAC) who underwent surgical intervention. Abbreviations: PDAC = Pancreatic Ductal Adenocarcinoma

imaging and a senior radiologist participated in the final decision. Disease-free survival (PFS) was defined as the time from the initial surgery to first-documented tumor recurrence (unequivocal radiological and/or histologic identification of PDAC) or all-cause death. Overall survival (OS) was defined as the time from the initial surgery to death of any cause.

Transformer model for prediction of LN metastasis

The flowchart of transformer model construction was shown in Fig. 2. We selected the ROI containing targeted tumor, pancreatic glands and adjacent areas from venous phase of the two types of DECT images including 100 keV, and 150 keV. Then, the size of each ROI was modified and normalized into 224 × 224 pixels. An in-house signatures extraction software with algorithms implemented in Visual Studio Code was used for DECT imaging processing. Three slices in ROI of DECT 100 keV, and 150 keV per patients were input synchronously transformer-based model. Detailed information on the mechanisms of transformer-based models, bidirectional multimodal attention and self-attention can be found in supplementary Materials E1.4 and experiments. To confirm the predictive performance of transformer-based model, we compared it with traditional LN CNNs [18].

In addition, we used multivariate logistic regression with forward stepwise for analysis of clinical data including DECT parameters, DECT reports, demographics data and laboratory findings.

Statistical analysis

The transformer-based model generated risk scores for LNM and low- and high-risk groups were distinguished using X-title soft. We compared survival outcomes between two risk groups by the Kaplan–Meier method and compared with the log-rank test. The hazard ratios (HRs) to compare survival between the two groups, with 95% confidence intervals (CIs) used to evaluate the variation around the estimated risk of events.

Uni- and multivariable regression analyses were conducted to identify independent clinical risk factors for LNM. Then, we will build a nomogram that integrated clinical information, DECT parameters and signatures. Although, we didn't perform sample-size calculation beforehand, according to the "ten events per variable" rule of thumb (LNM-positive, $n = 65$) in the nomogram, implying sufficient accuracy of the regression estimates. The clinical utility of the nomogram was evaluated with decision curve analysis (DCA).

The discrimination of different models was measured with the concordance area under the receiver

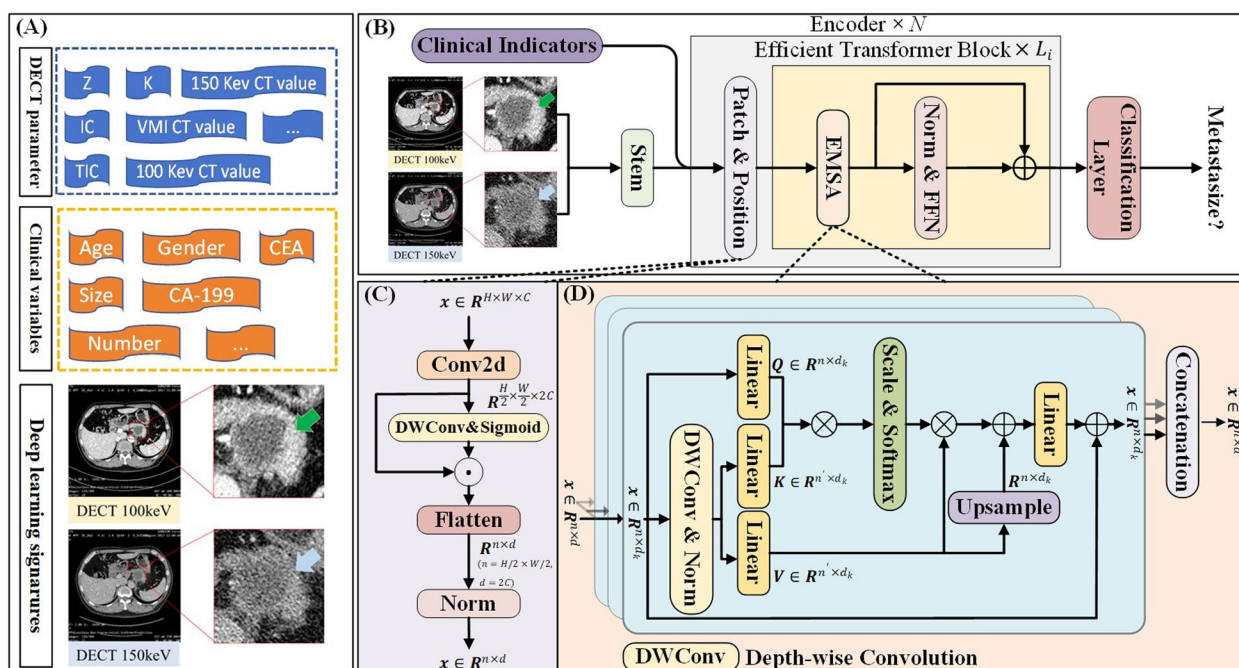


Fig. 2 Schematic representation of the workflow for the ViT (Vision Transformer) model, which utilizes Dual-energy Computed Tomography (DECT) to assess Lymph Node Metastases (LNM) in patients diagnosed with PDAC. **A** Data collect; **B** Data input the ViT (Vision Transformer) model and output LNM; **C-D** The computational architecture diagram of the ViT model. Abbreviations: DECT = Dual-energy Computed Tomography; LNM = Lymph Node Metastases; PDAC = Pancreatic Ductal Adenocarcinoma

operating characteristic curve (AUC) and compared by using Delong test. To explain DL models, the gradient-weighted class activation mapping (GRAD-CAM) was used to generate a rough location heat map highlighting the entry area of the classification target [19].

Statistical analysis was performed using SPSS version 23.0 (IBM Corp., NY, USA) and the “RMS package” using R software version 4.3.0 (<http://www.r-project.org/>). All tests of significance were two-sided, and $P < 0.05$ were considered statistically significant.

Results

Patient baseline characteristics

Table 1 outlined the PDAC patients’ baseline characteristics stratified by LN status at two sets. All variables’ baseline characteristics demonstrated a superior balance and consistency in the training set (all, $P > 0.05$). Notably, an older age was found to be more prevalent in the LNM-positive group than that in the LNM-negative group ($P = 0.015$) in the test set. Moreover, a higher tumor stages were shown in the LNM-positive group (T stage, $P < 0.001$; N stage $P = 0.011$). The LNM rates were 40.6% (65/160) in the training set, and 49.2% (31/63) in the test set, respectively, showing no significant difference between two sets ($P = 0.244$). 17.5% (28/160) patients received AT in the training set, and 14.3% (9/63) in the test set, respectively, showing no significant difference between two sets ($P = 0.561$).

The DECT parameters comparison between LNM-positive and negative group

The DECT parameters were compared between the LNM-positive group and the LNM-negative group in two sets and outlined in Table 2. Except for DECT parameters including IC, DIC and Z obtained from tumor region (both, $P < 0.001$ and 0.029) with statistical differences between two groups in the training set, others have no significant difference. Similar results are also found in the test set (both, $P < 0.001$ and 0.015). DECT parameters distribution and correlation were shown in Figure S1.

Multivariate cox regression analysis for LNM

Multivariate logistic regression of forward stepwise method found four independent risk factors significantly associated with LNM in the training set (Table 3), including tumor size (OR: 0.858; 95% CI: 0.766, 0.961; $P = 0.008$), DECT-reported LN status (OR: 2.535; 95% CI: 1.800, 3.570; $P < 0.001$), CA-199 (OR: 1.002; 95% CI: 1.000, 1.004; $P = 0.014$), and glucose (OR: 1.112; 95% CI: 1.046, 1.148; $P = 0.001$). Then, we added the DL signatures into these clinical variables and multivariate logistic regression of forward stepwise method showed DL signatures, high-risk score (OR: 7.082; 95% CI: 4.785–14.118;

$P < 0.001$), DECT-reported LN status (OR: 3.131; 95% CI: 2.142, 4.523; $P < 0.001$), CA-199 (OR: 1.004; 95% CI: 1.002, 1.006; $P < 0.001$), IC (OR: 0.213; 95% CI: 0.120, 0.476; $P < 0.001$), and Z (OR: 5.483; 95% CI: 2.204, 14.238; $P = 0.001$).

The development of transformer-based DL model

The AUC, SENS, SPEC, PPV, NPV and F1 score of DECT reports, clinical and each Vision Transformer (ViT) model based on DECT are outlined in Table 4. The ViT model’s performance outperforming other CNNs model including Resnet50, InceptionV3, VGG16, and Mobile Net was found (Table S1). The ICC of DECT reports by two radiologists were 0.84 in the training set and 0.80 in the test set, providing a common AUC value (0.62, 95% CI: 0.32–0.73) in the training set and (0.60, 95% CI: 0.45–0.73) in the test set, respectively. Clinical model that integrates DECT parameters and clinical variables slightly improved AUC than DECT reports with no statistical significance. Three transformer models based on DECT images including 100 keV model, 150 keV model, and 100 + 150 keV were compared. The results found that 100 + 150 keV DECT models yield the optimal performance among three models, with AUC: 0.94 (95% CI: 0.90–0.96) in the training set and 0.91 (95% CI: 0.75–1.00) in the test set.

Further, an integrated model was built based on these independent factors to predict LNM. Patients who received one individualized grade and higher total points of the assigned number had a LNM risk. The integrated model yields the best performance (0.94, 95% CI: 0.90–0.98 in the training set and 0.93, 95% CI: 0.84–1.00 in the test set) and showed a significantly better performance than the DECT reports, given by two radiologists, the model based on clinical variables, 100 keV model, and 150 keV model, in the test set (both, $P < 0.001$) according to the DeLong test. The AUC comparison between DECT-reports, clinical model, 100 keV model, 150 keV model, 100 + 150 keV model and integrated model were shown in two sets (Fig. 3).

Interpretation for transformer-based DL model

The ViT model-computed LNM risk score distribution of the test sets as well as four examples gradient-weighted class activation mapping of the original DECT images are shown in Fig. 4, which demonstrates a regular phenomenon with similar appearance in 100 keV and 150 keV DECT images. The density of red areas in the LNM-positive patients was higher than that in the LNM-negative patients. In addition, ViT models yield the most attentions (red areas) to pancreatic tissues surrounding the target tumor area instead of the tumor-self. This performance indicated that ViT models can visually display

Table 1 Baseline characteristics comparison between negative and positive for LNM in the primary and test sets

Variable	Primary dataset (n = 160)		P value	Test dataset (n = 63)		P value
	Negative for LNM (n = 95)	Positive for LNM (n = 65)		Negative for LNM (n = 32)	Positive for LNM (n = 31)	
Demographics						
Age (y), mean ± SD	57.4 ± 13.6	58.2 ± 10.3	0.689	55.4 ± 7.9	59.5 ± 8.8	0.015
Gender			0.790			0.513
Female	55 (57.9)	39 (59.6)		17 (53.1)	19 (61.3)	
Male	40 (42.1)	26 (40.4)		15 (46.9)	12 (38.7)	
Marital status			0.809			0.681
Unmarried	19 (20.0)	12 (18.5)		4 (12.5)	5 (16.1)	
Married	76 (80.0)	53 (81.5)		28 (87.5)	26 (83.9)	
Residence			0.753			0.674
Rural	40 (42.1)	29 (44.6)		13 (40.6)	11 (35.5)	
Urban	55 (57.9)	36 (55.4)		19 (59.4)	20 (64.5)	
Education			0.620			0.208
Low	17 (18.0)	11 (16.9)		7 (19.4)	6 (22.2)	
Medium	68 (71.6)	43 (66.2)		19 (63.9)	18 (59.3)	
High	10 (10.4)	7 (10.9)		6 (16.7)	7 (18.5)	
KPS			0.388			1.000
≤ 80	23 (24.2)	12 (18.5)		4 (3.6)	3 (3.4)	
> 80	72 (75.8)	53 (81.5)		28 (96.4)	28 (96.6)	
Comorbidities			0.661			0.355
Absence	81 (78.7)	57 (71.2)		31 (96.9)	28 (96.6)	
Presence	14 (21.3)	8 (28.8)		1 (3.1)	3 (3.4)	
Histologic grade			0.489			0.378
Well differentiated	68 (75.2)	48 (78.9)		17 (36.9)	15 (12.5)	
Moderately differentiated	12 (16.5)	7 (13.5)		11 (57.9)	14 (75.0)	
Poorly differentiated	15 (9.8)	10 (7.7)		4 (31.6)	2 (12.5)	
CT report						
Tumor size (cm), mean ± SD	3.4 ± 1.8	3.3 ± 1.1	0.637	3.3 ± 1.6	3.1 ± 1.0	0.550
Tumor number			1.000			1.000
Single	93 (96.7)	65 (100)		31 (100)	31 (100)	
Multiple	2 (3.3)	0 (0)		1 (0)	0 (0)	
Location			0.958			0.294
Head	61 (64.2)	40 (61.6)		22 (68.8)	22 (71.0)	
Neck	10 (10.5)	6 (9.2)		3 (9.3)	2 (6.4)	
Body	7 (7.4)	6 (9.2)		4 (12.5)	4 (12.8)	
Tail	17 (17.9)	13 (20.0)		3 (9.3)	3 (9.7)	
T stage			0.002			< 0.001
cT _a -cT ₂	50 (77.0)	18 (2.0)		26 (81.3)	10 (32.3)	
cT ₃ -cT ₄	45 (23.0)	47 (75.0)		6 (18.7)	21 (67.7)	
LN status			0.003			0.011
cN ₁ - 3	21 (30.6)	29 (59.6)		5 (15.6)	14 (46.2)	
cN ₀	74 (69.4)	36 (40.4)		27 (74.4)	17 (53.8)	
Metastasis			0.939			1.000
cM ₁	7(9.8)	5 (1.9)		3 (9.3)	2 (9.7)	
cM ₀	88 (90.2)	60 (98.1)		29 (90.7)	29 (90.3)	
Laboratory findings						
Median CA- 199 (U/L) ^a	409.2 (22.6, 18,485.2)	983.5(42.5, 22,378.8)	< 0.001	248.4 (6.6, 2423.5)	489.8 (7.4, 908.6)	< 0.001
Median CEA9 (U/L) ^a	4.8 (1.6, 83.3)	16.2 (5.4, 78.2)	0.089	2.6 (0.9, 66.9)	10.9 (3.9, 75.8)	< 0.001

Table 1 (continued)

Variable	Primary dataset (n = 160)		P value	Test dataset (n = 63)		P value
	Negative for LNM (n = 95)	Positive for LNM (n = 65)		Negative for LNM (n = 32)	Positive for LNM (n = 31)	
Glucose, mean ± SD (mmol/L) ^a	7.1 ± 2.9	7.1 ± 2.5	0.970	7.4 ± 2.2	7.6 ± 2.0	0.874
Median GGT (U/L) ^a	280.3 (32.2, 2343.9)	221.1(12.5, 2126.7)	0.361	193.1 (17.0, 1847.2)	385.6 (22.3, 683.2)	0.415
Median Total bilirubin (μmol/L) ^a	73.5 (22.1, 334.2)	76.6 (16.3, 290.2)	0.804	44.7 (16.0, 424.2)	62.2 (15.1, 185.5)	0.256
NAT			0.924			0.906
Absence	78(82.1)	54 (83.1)		27 (84.3)	27 (87.1)	
Presence	17 (17.9)	11(16.9)		5 (15.7)	4 (12.9)	
Median progression-free survival, months ^a	6.5 (2.1, 9.2)	4.6 (1.2, 8.5)	< 0.001	5.7 (1.8, 8.2)	4.3 (1.0, 7.5)	< 0.001
Median overall survival, months ^a	11.5 (4.5, 17.4)	8.2 (3.3, 15.4)	< 0.001	10.8 (5.8, 18.4)	7.3 (4.2, 17.9)	< 0.001

Data are number of patients; data in parentheses are percentage unless otherwise indicated

Abbreviation: LNM lymph node metastases, CT computed tomography, KPS karnofsky performance score, CA 19-9 carbohydrate antigen 19-9, CEA carcino-embryonic antigen, GGT γ-glutamyl transpeptidase, NAT neoadjuvant treatment

^a Data in parentheses are interquartile range

Table 2 DECT Parameter Comparison Between Negative and Positive for LNM in the Primary and Test sets

DECT parameters	Traning dataset (n = 160)		P value	Test dataset (n = 63)		P value
	Negative for LNM (n = 95)	Positive for LNM (n = 65)		Negative for LNM (n = 32)	Positive for LNM (n = 31)	
Tumor region ^a						
ROI cm ²	0.50 ± 0.10	0.50 ± 0.11	0.908	0.50 ± 0.14	0.50 ± 0.15	0.772
100 keV CT value (Hu)	97.8 ± 36.1	99.6 ± 33.4	0.782	99.2 ± 21.3	108.6 ± 23.5	0.789
150 keV CT value (Hu)	62.7 ± 17.5	57.8 ± 14.0	0.589	61.3 ± 14.6	62.9 ± 11.8	0.672
VMI 40 keV (Hu)	223.4 ± 92.1	226.5 ± 102.0	0.920	277.6 ± 48.9	266.8 ± 32.6	0.578
VMI 70 keV(Hu)	91.6 ± 21.6	90.0 ± 21.2	0.982	90.5 ± 22.3	99.6 ± 31.0	0.514
K value	4.4 ± 0.5	4.5 ± 0.9	0.955	4.8 ± 0.7	4.1 ± 0.5	0.674
IC (mg/ml)	2.3 ± 0.8	4.2 ± 1.1	< 0.001	2.2 ± 0.9	4.2 ± 0.4	< 0.001
NIC (%)	32.1 ± 6.3	45.2 ± 9.6	< 0.001	32.9 ± 13.7	43.8 ± 13.7	< 0.001
Rho	37.0 ± 6.2	48.4 ± 8.5	0.356	32.9 ± 7.2	36.7 ± 9.9	0.220
Z	8.2 ± 0.5	8.6 ± 0.4	0.029	8.4 ± 0.3	8.7 ± 0.4	0.045
DEI	0.017 ± 0.002	0.018 ± 0.004	0.854	0.017 ± 0.005	0.018 ± 0.006	0.885
Pancreatic region ^a						
ROI cm ²	0.50 ± 0.10	0.50 ± 0.11	0.911	0.50 ± 0.12	0.50 ± 0.14	0.788
100 keV CT value (Hu)	96.4 ± 38.2	93.6 ± 23.4	0.667	82.7 ± 19.0	112.0 ± 41.3	0.612
150 keV CT value (Hu)	56.7 ± 18.1	57.7 ± 13.1	0.740	57.7 ± 12.3	61.9 ± 14.2	0.212
VMI 40 keV (Hu)	223.0 ± 103.6	213.2 ± 79.2	0.575	176.7 ± 48.9	218.3 ± 55.6	0.420
VMI 70 keV (Hu)	91.3 ± 34.0	89.2 ± 24.0	0.721	81.8 ± 25.5	104.3 ± 36.4	0.050
K value	4.4 ± 2.4	4.1 ± 1.7	0.523	5.0 ± 2.0	6.1 ± 1.9	0.263
IC (mg/ml)	2.4 ± 1.3	2.3 ± 1.0	0.599	2.7 ± 0.8	2.7 ± 0.4	0.090
NIC (%)	32.9 ± 13.7	33.8 ± 13.7	0.716	32.9 ± 13.7	33.8 ± 13.7	0.716
Rho	34.8 ± 9.8	36.4 ± 8.1	0.356	34.8 ± 9.8	36.4 ± 8.1	0.056
Z	8.6 ± 0.3	8.6 ± 0.4	0.975	8.2 ± 0.5	7.7 ± 0.8	0.271
DEI	0.018 ± 0.009	0.016 ± 0.007	0.567	0.014 ± 0.005	0.020 ± 0.017	0.125

Abbreviation: ROI: region of interest; VMI: virtual monoenergetic images; Z: atomic number; IC: iodine content; Rho: electron cloud density; DEI: dual-energy index

^a Scanning in venous phase.K value = (HU40keV-HU70keV)/30

Table 3 Stepwise Multivariable Logistic Regression Analysis for Factors Associated with Odds of LNM of PDAC in the Training set

Variable	Clinical-DECT parameters				Clinical-DECT parameters-DL signatures			
	β	Wald	OR (95% CI)	P value	β	Wald	OR (95% CI)	P value
Tumor size (cm), (per 0.1 increase)	-.153	.058	.858 (.766-.961)	.008				
Glucose (mmol/L), (per 0.1 increase)	.106	.031	1.112 (1.046–1.148)	.001				
CA- 199 (μmol/L), (per 0.1 increase)	.002	.001	1.002 (1.000–1.004)	.014	.004	.001	1.004 (1.002–1.006)	<.001
DECT report of LNM, presence	.930	.175	2.535 (1.800–3.570)	<.001	1.136	.191	3.131 (2.142–4.523)	<.001
DL signatures, high-risk score					2.236	.329	7.082 (4.785–14.118)	<.001
100 keV CT value (Hu), (per 0.1 increase)								
150 keV CT value (Hu), (per 0.1 increase)								
VMI 40 keV (Hu), (per 0.1 increase)								
VMI 70 keV(Hu), (per 0.1 increase)								
K value, (per 0.1 increase)								
IC (mg/ml), (per 0.1 increase)					– 1.546	.294	.213 (.120-.476)	<.001
NIC (%), (per 0.1 increase)					NA	NA		
Rho, (per 0.1 increase)					NA	NA		
Z, (per 0.1 increase)					1.702	.509	5.483 (2.204–14.238)	.001
DEI, (per 0.1 increase)					NA	NA		

These analyses were performed using the training cohort (n = 160). Numbers in parentheses are 95% CIs

Abbreviation: PDAC pancreatic ductal adenocarcinoma, LNM lymph node metastases, DECT dual-energy computed tomography, VMI virtual monoenergetic images, Z atomic number, IC iodine content, Rho electron cloud density, DEI dual-energy index, NA

Table 4 The performance comparison of different models

Models	Cohorts	AUC	ACC	SENS	SPEC	PPV	NPV
DECT reports	Training	0.62 (0.32,0.73)	0.64 (0.45,0.78)	0.70 (0.33,0.83)	0.59 (0.40,0.70)	0.61 (0.49,0.73)	0.66 (0.48,0.75)
	Test	0.60 (0.45,0.73)	0.60 (0.50,0.67)	0.67 (0.49,0.82)	0.53 (0.47,0.77)	0.60 (0.41,0.75)	0.50 (0.27,0.75)
Clinical	Training	0.66 (0.32,0.73)	0.62 (0.27,0.58)	0.68 (0.53,0.83)	0.59 (0.40,0.70)	0.61 (0.49,0.73)	0.56 (0.58,0.75)
	Test	0.63 (0.55,0.73)	0.61 (0.50,0.75)	0.57 (0.49,0.72)	0.53 (0.47,0.77)	0.55 (0.41,0.75)	0.52 (0.47,0.75)
100 keV ViT	Training	0.94 (0.84,1.00)	0.87 (0.73,0.97)	0.79 (0.56,1.0)	0.94 (0.78,1.00)	0.92 (0.73,1.00)	0.83 (0.64,1.00)
	Test	0.73 (0.54,0.92)	0.70 (0.55,0.85)	0.87 (0.67,1.0)	0.56 (0.33,0.78)	0.62 (0.41,0.81)	0.83 (0.60,1.00)
150 keV ViT	Training	0.95 (0.90,0.97)	0.88 (0.82,0.93)	0.87 (0.78,0.95)	0.88 (0.80,0.95)	0.87 (0.77,0.95)	0.88 (0.79,0.95)
	Test	0.84 (0.70,0.96)	0.73 (0.57,0.87)	0.71 (0.47,0.93)	0.75 (0.50,0.94)	0.71 (0.50,0.93)	0.75 (0.53,0.94)
100 + 150 keV ViT	Training	0.94 (0.90,0.96)	0.89 (0.84,0.94)	0.90 (0.82,0.97)	0.88 (0.80,0.95)	0.87 (0.79,0.95)	0.91 (0.84,0.97)
	Test	0.91 (0.75,1.00)	0.90 (0.77,1.00)	0.86 (0.67,1.00)	0.94 (0.79,1.00)	0.92 (0.75,1.00)	0.88 (0.71,1.00)
ViT + clinical model	Training	0.94 (0.90,0.98)	0.90 (0.84,0.95)	0.88 (0.80,0.96)	0.91 (0.83,0.97)	0.90 (0.82,0.97)	0.90 (0.82,0.97)
	Test	0.93 (0.84,1.00)	0.83 (0.70,0.97)	0.86 (0.67,1.00)	0.81 (0.62,1.00)	0.80 (0.58,1.00)	0.87 (0.67,1.00)
Cohorts	DECT reports		Clinical		100 keV	150 keV	100 + 150 keV
Test [#]	< 0.001		< 0.001		< 0.001	< 0.001	0.265

Numbers in parentheses are the 95% confidence interval. The bold values represent the optimal AUC value

AUC areas under receiver operating characteristic curve, ACC accuracy, SENS sensitivity, SPEC specificity, PPV positive predictive value, NPV negative predictive value

[#] Comparison between DL based nomogram and other models using significant level of Delong test for methods

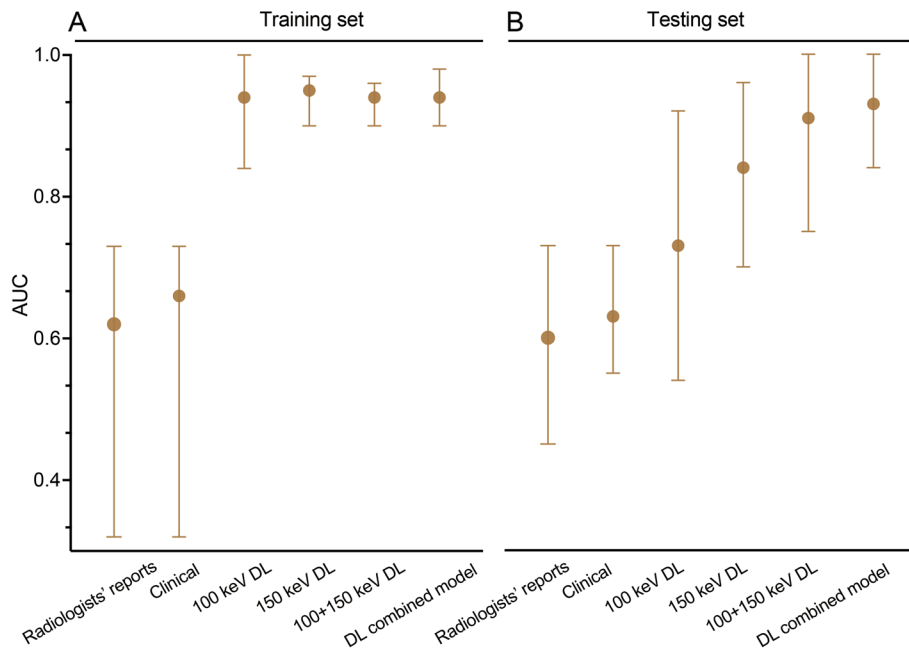


Fig. 3 A nomogram calibrated by the coefficients of various risk factors to forecast lymph node metastases (LNM). The nomogram is defined by the equation: $Y = -8.796 + 3.023 \times Z + 1.528 \times CA - 199 + 2.027 \times IC + 4.561 \times CT\text{-reports} + 6.961 \times \text{Risk scores}$, where Y represents the probability of LNM in PDAC patients. The calibration curve illustrates the alignment of the model's predictions with the actual observed probabilities in both the (B) training set and (C) test set. The decision curve analysis (DCA) revealed that the nomogram exhibited superior net benefit across a spectrum of reasonable threshold probabilities in both the training (D) and test set (E). Abbreviations: LNM = Lymph Node Metastases; PDAC = Pancreatic Ductal Adenocarcinoma; DCA = Decision Curve Analysis

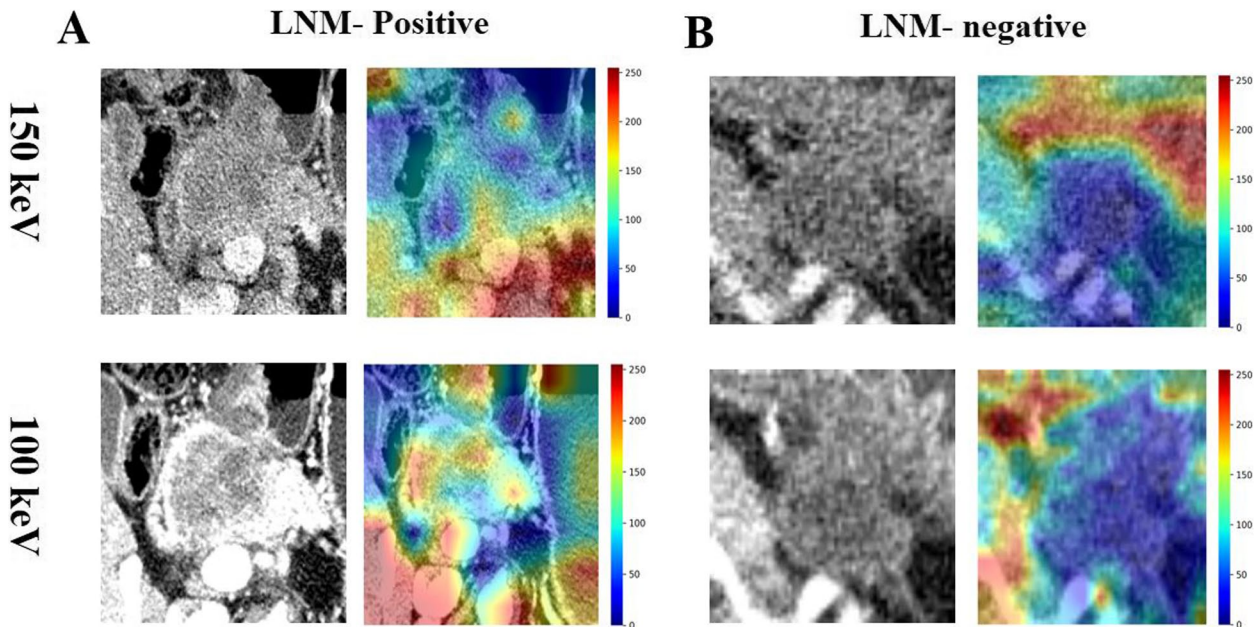


Fig. 4 Illustrates the comparison of receiver operating characteristic (ROC) curves for various models predicting LNM in PDAC, across both the training set (A) and the test set (B). Abbreviations: LNM = Lymph Node Metastases; PDAC = Pancreatic Ductal Adenocarcinoma

the areas where lymph nodes are prone to metastasis and to distinguish out LNM status, even if above-mentioned areas did not attract the attention of radiation experts. Notably, ViT models sought different adjacent areas of PDAC for the same patient, which explained why they provided different predictive performances.

Association between transformer-predicted lnm status and survival

To facilitate the clinical practice of the nomogram, we divided PDAC patients into two groups according to the LNM risk scores, including a high-risk group and low-risk group. We identified the cut-off values (22.18) in the PC and verified them in the TC. The median follow-up duration was 22.5 months (IQR, 14.2–30.8 months) in

the LNM-negative group and 20.4 months (IQR, 13.7–28.4 months) in the LNM-positive group. According to the cut-off values of LNM risk scores, the 1-, 2- and 3-years OS were 85.6%, 70.2% and 54.8%, respectively, in the low-risk group and the 1-, 2- and 3-years OS were 55.6%, 31.2% and 24.8%, respectively, in the high-risk group, showing significant statistical difference in the training set ($P < 0.001$) (Figs. 5A). Similarly, the cumulative 1-, 2-, and 3-year OS rates among the high-risk and low-risk groups were also significant difference in the test set ($P = 0.023$) (Fig. 5B). The 1-, 2- and 3-year PFS were 56.5%, 50.2% and 37.5%, respectively, in the low-risk group, which was better than that in high-risk group (53.2%, 12.4% and 12.4%, respectively) in the training set ($P = 0.016$) (Fig. 5C). Similarly, the cumulative 1-, 2-, and

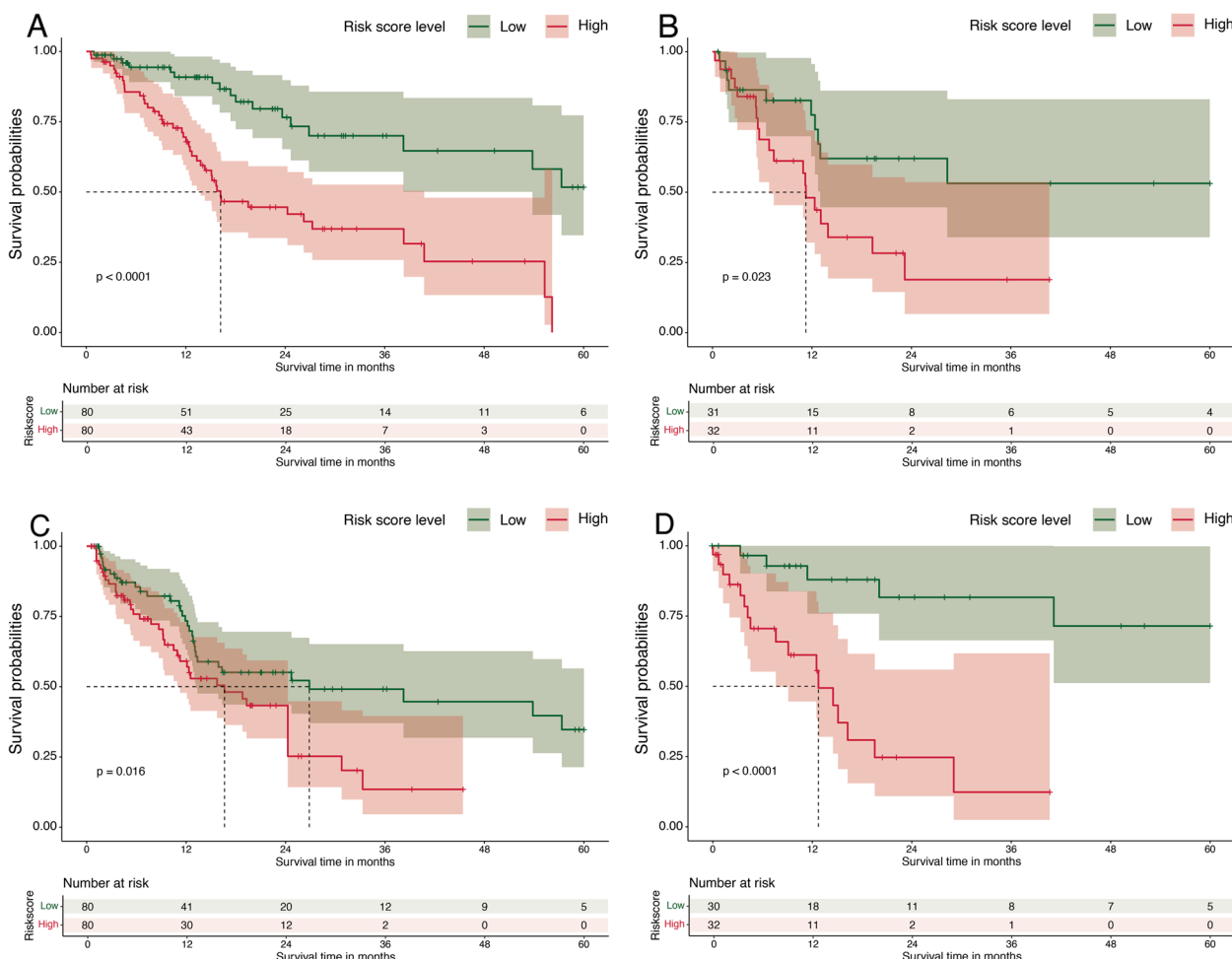


Fig. 5 provides a visual representation of two PDAC patient examples, displaying dual-energy computed tomography (DECT) imaging at 100 keV and 150 keV, along with corresponding heat maps. The red regions indicate areas of greater weight, which can be interpreted using the color bar on the right. **A** Depicts a 52-year-old male PDAC patient with LNM, who has a poor prognosis and a median overall survival (OS) of 7.8 months. **B** Shows a 48-year-old female PDAC patient without LNM, who has a favorable prognosis and a median OS of 15.9 months. Abbreviations: LNM = Lymph Node Metastases; PDAC = Pancreatic Ductal Adenocarcinoma; OS = Overall Survival; DECT = Dual-energy Computed Tomography

3-year PFS rates among the high-risk and low-risk groups were also significant difference in the test set ($P < 0.001$) (Fig. 5D).

The Subgroup analysis

ViT model-predicted LNM risk was a strong predictor for OS and PFS in different subgroups in two sets (Table S2). Conventional metrics including age, gender, tumor size, CA-199, and NAT, based on a subset of patients with PDAC. Similar survival comparison between two risk groups were observed in the above-mentioned subgroup using forest plots (Figure S2).

Discussion

The integrated model based on ViT algorithm contributed to help physicians identifying whether there is a LNM for PDAC patients and developing corresponding decision-making plans. Previous studies have investigated various risk identification methods for LNM [9, 20, 21], but so far, preoperative distinguish of LNM still mainly depends on the radiologist's reports. A low AUC value of 0.60 from radiologists' reports in the test set was found in our study. Even if these radiologists used DECT parameters to help identify LNM, the predictive performance of DECT reports remains struggling to achieve significant improvement. Notably, we select the ROIs of tumor and pancreas to obtain the DECT parameters, but the results found that IC and Z have significant statistical difference between LNM-positive and negative group, indicating only special DECT parameters contributed to identifying the LNM based on significant improvement of image quality and tumor differentiation.

To date, several studies have assessed preoperatively LNM using artificial intelligence (AI) algorithm in PDAC patients. For example, Shao et al developed and validated an AI model using cropped sub volume centered LN instances at CT to identify automatically segmented LNs as positive or negative metastasis [22]. The model provided a well-received AUC value of 0.91 in the training set and 0.92 in the validation set, respectively. However, the primary limitation of this study was the target tumor and LN need to manual sketch to train and extract signatures. This requires a lot of time and effort from radiologists. Another limitation of these similar studies were that the radiomics features or signatures extracted from ROI using AI model were difficult to achieve consistency from one another, indicating a challenge for reproducibility [23, 24].

Given the high-contrast and multi-parameter characteristics of DECT imaging, we attempted to build ViT models using various DECT imaging, including 100 keV, 150 keV and 100 keV plus 150 keV. We found that the signatures synchronously extracted from 100 and 150

keV DECT imaging and input into the ViT model, so the LNM predictive performance of final output is the best among three ViT models. This result suggests that the signatures extracted from the 100 and 150 keV DECT images have complementary information, which can help the ViT model improving its ability to distinguish LNM. On this basis, two key DECT parameters including Z and IC, combined with DECT reports and CA-199 as an important PDAC' biomarker was added into ViT 100 + 150 keV risk scores to build an integrated model for prediction LNM of PDAC. It turns out that the performance of the integrated model was slightly improved than that of ViT 100 + 150 keV model. The integrated mode demonstrated favorable discrimination in both the training set (AUC, 0.94) and the test set (AUC, 0.93), outperforming radiologists' reports, and clinical model (DeLong test, both, $P < 0.001$). Further, the PDAC patients with LNM identified by the integrated model yielded an approximately 50% worse survival who underwent radical resection, thereby providing important prompt information for decision-making support.

We hypothesized that ViT model as the network backbone can obtain more DECT information than CNNs model [25–27]. Therefore, we conducted a preliminary experiment comparing the predictive ability of AI models using various DL approaches. It was found that the ViT model indeed has better predictive performance than traditional CNNs. To our knowledge, ViT has not yet been widely used in medical image classification, let alone survival prediction. Previous studies have shown that transformer models were used to prognostic prediction of patients with rectal cancer based on MRI [28]. The model computed risk score was also able to accurately predict PFS at 1-, 3-, and 5- years in the validation set. In this study, we empirically demonstrated that the pretrained ViT can achieve better performance than traditional CNNs in terms of survival prediction, such as, predictive LNM AUC, 0.93 (ViT) vs. 0.72 (ResNet50); $P < 0.001$.

To interpret the ViT model, we used Grad CAM to visualize the region of LNM with a rough heat map. We simultaneously observed the heatmap distribution status of DECT images at 100 and 150 keV, and the results found that red color weight is mainly distributed in the peripheral area of the tumor in the LNM-positive group regardless of the location of PDAC tumor. For the same patient, the weight and distribution of heat maps in both the 100 and 150 keV groups are almost consistent, indicating that the ability of the ViT model to distinguish LNM is consistent in both modalities of DECT imaging. Notably, peripheral area of the tumor was more worthy of the attention of doctors than the intertumoral region, due to cancer cells that metastasize to the lymphatic system often spread along this pathway [29, 30].

This common phenomenon revealed the working principle of ViT models based on DECT imaging for identify LNM. Besides those, the visualization of extracted signatures on 100 and 150 keV DECT imaging directly demonstrated that tumor characteristics in hidden layers and indeed suggest the difference between LNM-negative and positive group, which was captured by ViT models.

Our results found that PDAC patients stratified into high- and low-risk LNM groups using the integrated model showed significantly different survival benefit including OS and PFS improvement. In addition, we found the NAT didn't interference with the prediction results of the integrated model according to the subgroup analysis. This ViT based integrated model help surgeons to develop a scheme after surgery. Multiple integrational guidelines suggest that NAT has been adopted as an important adjuvant treatment when enlarged LN around the pancreas are highly suspected of metastasis [31, 32]. Once the nomogram is used to identify LNM, NAT should be used in a timely manner.

There are certain limitations in our study. First, the ViT based integrated model remains to seem mildly overfitted due to the small sample size of this study. More DECT data of PDAC should be collected to further confirm the performance and the robustness of the ViT based integrated model. Second, we did not collect pathological and gene factors for improvement of survival outcomes prediction, and the importance of these factors should be investigated further. Third, there may have been difficulty in correlating LNs obtained at surgery with the specific nodes seen at preoperative scanning, representing a potential limitation. Finally, we did not evaluate the benefit of AT and postoperative chemotherapy for patients with PDAC.

In conclusion, the ViT based integrated model that integrated clinical information, DECT parameters and DL-signatures exhibited outstanding performance in predicting LNM of PDAC patients. This novel AI model may help surgeons for individualized therapeutic decision-making in PDAC for clinical practice and trials. Further, a prospective clinical trial should be designed to obtain power and reliable evidences.

Abbreviations

AUC	Area under the curve
CA- 199	Carbohydrate antigen- 199
DECT	Dual-energy computed tomography
PDAC	Pancreatic ductal adenocarcinoma
PFS	Progression-free survival
NAT	Neoadjuvant chemotherapy

Supplementary Information

The online version contains supplementary material available at <https://doi.org/10.1186/s12957-025-03774-6>.

Supplementary Material 1.

Acknowledgements

The authors acknowledge and express their deepest gratitude to the participants of this study.

Authors' contributions

X.D. and X.W. wrote the main manuscript text and L.G. prepared figures 1 - 3. All authors reviewed the manuscript.

Funding

This work was supported by the Comprehensive research project (KJ2023 C0 KYD05), Medical center boosting project of Air Force Medical Center (2022ZTJB01).

Data availability

No datasets were generated or analysed during the current study.

Declarations

Ethics approval and consent to participate

This retrospective study obtained approval of the institutional review board of Qingdao Central Hospital (B2019 - 012-01).

Consent for publication

Not applicable.

Competing interests

The authors declare no competing interests.

Author details

¹Department of Interventional Radiology, Qingdao Central Hospital, University of Health and Rehabilitation Sciences (Qingdao Central Hospital), Qingdao, Shandong 266042, China. ²Department of Oncology, Qingdao Hospital, University of Health and Rehabilitation Sciences (Qingdao Municipal Hospital), Qingdao, Shandong 266071, China. ³Department of Oncology, Qingdao Central Hospital, University of Health and Rehabilitation Sciences (Qingdao Central Hospital), Qingdao, Shandong 266042, China. ⁴Department of Interventional Radiology, Qingdao Central Hospital, University of Health and Rehabilitation Sciences (Qingdao Central Hospital), Qingdao, Shandong 266000, China.

Received: 15 November 2024 Accepted: 23 March 2025

Published online: 09 April 2025

References

- Bray F, Laversanne M, Sung H, et al. Global cancer statistics 2022: GLOBOCAN estimates of incidence and mortality worldwide for 36 cancers in 185 countries. *CA Cancer J Clin*. 2024;74(3):229–63. <https://doi.org/10.3322/caac.21834>.
- Rahib L, Smith BD, Aizenberg R, Rosenzweig AB, Fleshman JM, Matrisian LM. Projecting cancer incidence and deaths to 2030: the unexpected burden of thyroid, liver, and pancreas cancers in the United States. *Cancer Res*. 2014;74(11):2913–21. <https://doi.org/10.1158/0008-5472.CAN-14-0155>.
- Hopstaken JS, Daamen LA, Patijn GA, et al. ATionwide evaluation of pancreatic cancer networks ten years after the centralization of pancreatic surgery. *HPB (Oxford)*. 2023;25(12):1513–22. <https://doi.org/10.1016/j.hpb.2023.07.904>.
- Martin D, Alberti P, Wigmore SJ, Demartines N, Joliat GR. Pancreatic Cancer Surgery: What Matters to Patients. *J Clin Med* 2023;12(14). <https://doi.org/10.3390/jcm12144611>.
- Pentheroudakis G, ESMO Guidelines Committee. Recent eUpdates to the ESMO Clinical Practice Guidelines on hepatocellular carcinoma, cancer of the pancreas, soft tissue and visceral sarcomas, cancer of the prostate and gastric cancer. *Ann Oncol* 2019;30(8):1395–1397. <https://doi.org/10.1093/annonc/mdz180>.
- Noda Y, Goshima S, Kawada H, et al. Modified ATional Comprehensive Cancer Network Criteria for Assessing Resectability of Pancreatic Ductal Adenocarcinoma. *AJR Am J Roentgenol*. 2018;210(6):1252–8. <https://doi.org/10.2214/AJR.17.18595>.

7. Garcés-Descovich A, Beker K, Jaramillo-Cardoso A, James Moser A, Mortelet KJ. Applicability of current NCCN Guidelines for pancreatic adenocarcinoma resectability: analysis and pitfalls. *Abdom Radiol (NY)*. 2018;43(2):314–22. <https://doi.org/10.1007/s00261-018-1459-6>.
8. Wang B, Zhang K, Ding Y, Huang T. Diagnostic value of multi-slice spiral CT and MRI in peripheral lymph node metastasis of pancreatic cancer. *Asian J Surg*. 2023;46(5):2083–4. <https://doi.org/10.1016/j.asjsur.2022.11.034>.
9. Masuda T, Dann AM, Elliott IA, et al. A Comprehensive Assessment of Accurate Lymph Node Staging and Preoperative Detection in Resected Pancreatic Cancer. *J Gastrointest Surg*. 2018;22(2):295–302. <https://doi.org/10.1007/s11605-017-3607-7>.
10. Somers I, Bipat S. Contrast-enhanced CT in determining resectability in patients with pancreatic carcinoma: a meta-analysis of the positive predictive values of CT. *Eur Radiol*. 2017;27(8):3408–35. <https://doi.org/10.1007/s00330-016-4708-5>.
11. Li Q, Xu WY, Sun NN, et al. MRI versus Dual-Energy CT in Local-Regional Staging of Gastric Cancer. *Radiology*. 2024;312(1):e232387. <https://doi.org/10.1148/radiol.232387>.
12. Li M, Fan Y, You H, et al. Dual-Energy CT Deep Learning Radiomics to Predict Macrotrabecular-Massive Hepatocellular Carcinoma. *Radiology*. 2023;308(2):e230255. <https://doi.org/10.1148/radiol.230255>.
13. Gruenewald LD, Koch V, Martin SS, et al. Dual-Energy CT-based Opportunistic Volumetric Bone Mineral Density Assessment of the Distal Radius. *Radiology*. 2023;308(2):e223150. <https://doi.org/10.1148/radiol.223150>.
14. An C, Li D, Li S, et al. Deep learning radiomics of dual-energy computed tomography for predicting lymph node metastases of pancreatic ductal adenocarcinoma. *Eur J Nucl Med Mol Imaging*. 2022;49(4):1187–99. <https://doi.org/10.1007/s00259-021-05573-z>.
15. Baid G, Cook DE, Shafin K, et al. DeepConsensus improves the accuracy of sequences with a gap-aware sequence transformer. *AT Biotechnol*. 2023;41(2):232–8. <https://doi.org/10.1038/s41587-022-01435-7>.
16. Wang W, Wang Y, Song D, et al. A Transformer-Based microvascular invasion classifier enhances prognostic stratification in HCC following radiofrequency ablation. *Liver Int*. 2024;44(4):894–906. <https://doi.org/10.1111/liv.15846>.
17. Cohen JF, Bossuyt P. TRIPOD+AI: an updated reporting guideline for clinical prediction models. *BMJ*. 2024;385:q824. <https://doi.org/10.1136/bmj.q824>.
18. Sun Q, Fang N, Liu Z, Zhao L, Wen Y, Lin H. HybridCTrm: Bridging CNN and Transformer for Multimodal Brain Image Segmentation. *J Healthc Eng*. 2021;2021:7467261. <https://doi.org/10.1155/2021/7467261>.
19. Zhang P, Yang L, Mao Y, et al. CorNet: Autonomous feature learning in raw Corvis ST data for keratoconus diagnosis via residual CNN approach. *Comput Biol Med*. 2024;172: 108286. <https://doi.org/10.1016/j.compbiomed.2024.108286>.
20. Nishiwada S, Sho M, Banwait JK, et al. A MicroRNA SigATURE Identifies Pancreatic Ductal Adenocarcinoma Patients at Risk for Lymph Node Metastases. *Gastroenterology*. 2020;159(2):562–74. <https://doi.org/10.1053/j.gastro.2020.04.057>.
21. Cheng H, Xu JH, Kang XH, et al. Nomogram for predicting the pre-operative lymph node metastasis in resectable pancreatic cancer. *J Cancer Res Clin Oncol*. 2023;149(13):12469–77. <https://doi.org/10.1007/s00432-023-05048-8>.
22. Bian Y, Zheng Z, Fang X, et al. Artificial Intelligence to Predict Lymph Node Metastasis at CT in Pancreatic Ductal Adenocarcinoma. *Radiology*. 2023;306(1):160–9. <https://doi.org/10.1148/radiol.220329>.
23. Fu N, Fu W, Chen H, et al. A deep-learning radiomics-based lymph node metastasis predictive model for pancreatic cancer: a diagnostic study. *Int J Surg*. 2023;109(8):2196–203. <https://doi.org/10.1097/JS9.00000000000000469>.
24. Xu X, Zhang HL, Liu QP, et al. Radiomic analysis of contrast-enhanced CT predicts microvascular invasion and outcome in hepatocellular carcinoma. *J Hepatol*. 2019;70(6):1133–44. <https://doi.org/10.1016/j.jhep.2019.02.023>.
25. Tang H, Liu S, Tan W, Fu L, Yan M, Feng H. Prediction of midpalatal suture maturation stage based on transfer learning and enhanced vision transformer. *BMC Med Inform Decis Mak*. 2024;24(1):232. <https://doi.org/10.1186/s12911-024-02598-w>.
26. Xu S, Chen Y, Yang S, Zhang X, Sun F. FCSU-Net: A novel full-scale Cross-dimension Self-attention U-Net with collaborative fusion of multi-scale feature for medical image segmentation. *Comput Biol Med*. 2024;180: 108947. <https://doi.org/10.1016/j.compbiomed.2024.108947>.
27. Arjmandi N, Nasser S, Momenzad M, et al. Automated contouring of CTV and OARs in planning CT scans using novel hybrid convolution-transformer networks for prostate cancer radiotherapy. *Discov Oncol*. 2024;15(1):323. <https://doi.org/10.1007/s12672-024-01177-9>.
28. Jiang X, Zhao H, Saldanha OL, et al. An MRI Deep Learning Model Predicts Outcome in Rectal Cancer. *Radiology*. 2023;307(5): e222223. <https://doi.org/10.1148/radiol.222223>.
29. Zourelidis A, Trojanowicz B, Sunami Y, Hause G, Vieweg D, Kleeff J. Distance-dependent transcriptome changes of pancreatic stellate cells in paracrine pancreatic ductal adenocarcinoma co-culture models. *Sci Rep*. 2024;14(1):18030. <https://doi.org/10.1038/s41598-024-68148-6>.
30. Binnewies M, Roberts EW, Kersten K, et al. Understanding the tumor immune microenvironment (TIME) for effective therapy. *AT Med*. 2018;24(5):541–50. <https://doi.org/10.1038/s41591-018-0014-x>.
31. Jung HS, Han Y, Yun WG, et al. Examining neoadjuvant treatment candidates in resectable pancreatic cancer based on tumor-vessel interactions and CA 19–9 levels: a retrospective set study. *Int J Surg*. 2024;110(5):2883–93. <https://doi.org/10.1097/JS9.0000000000001184>.
32. Stillger MN, Kurowski K, Bronsert P, et al. Neoadjuvant chemo- or chemo-radiation-therapy of pancreatic ductal adenocarcinoma differentially shift ECM composition, complement activation, energy metabolism and ribosomal proteins of the residual tumor mass. *Int J Cancer*. 2024;154(12):2162–75. <https://doi.org/10.1002/ijc.34867>.

Publisher's Note

Springer Nature remains neutral with regard to jurisdictional claims in published maps and institutional affiliations.